Trends in sputter yield data in the film deposition regime

John E. Mahan
Department of Electrical Engineering, Colorado State University, Fort Collins, Colorado 80523

André Vantomme
Instituut voor Kern en Stralingsfysika, Katholieke Universiteit Leuven, Celestijnenlaan 200D, B-3001 Leuven, Belgium
(Received 22 October 1998; revised manuscript received 25 October 1999)

Knowing the fundamental trends of sputter yield in the sputtering regime used for film deposition is crucial for understanding the mechanisms of sputter deposition, interpreting yield data, and predicting the results of experiments. One source of experimental yield data is the comprehensive compilation [N. Matsunami, Y. Yamamura, Y. Itikawa, N. Itoh, Y. Kazomata, S. Miyagawa, K. Morita, R. Shimizu, and H. Tawara, At. Data Nucl. Data Tables **31**, 1 (1984)]. They published graphical yield-energy curves based on empirical parameters which were best fits to nearly all the projectile-target combinations available in 1983. We interpret this experimental data using theoretical results from a ''simplified collisional model'' of sputtering. For 1-keV noble gas projectiles, several trends show forth (some old and some new): First, there is a repeating pattern in the dependence of yield on target atomic number, with the period being each row of the Periodic Table. Second, surface binding energy is the single most important target parameter; the yield varies roughly as $1/U_{sb}^{1.3}$ for the empirical data, but as $1/U_{sb}^{0.5}$ for the pure linear cascade sputtering mechanism. Third, while the principal mechanism is the linear cascade, the nonlinear cascade makes a detectable contribution to the experimental yield for yield values above ~1. Fourth, for target atomic numbers above ~35, the yield increases monotonically with projectile mass; for lighter targets the yield exhibits a maximum at an intermediate projectile mass. Fifth, the energy dependence of yield for a given projectile-target combination from ~0.5 to 2 keV is, to a good approximation, $Y(E)\propto E^{0.5}$. Scatter due to experimental error is evident in the data: Matsunami *et al.*'s approach of combining the results of different experiments, resulting in their empirical yield curves, is useful for compensating for this.

INTRODUCTION

There has long been a need for summaries of sputter yield data at projectile energies typical of thin film deposition (on the order of 1 keV), and for treatments of such data that address the problems of lack of consistency and poor experimental reproducibility.[1] The objectives include obtaining reliable predictions of yield, and understanding the phenomena of sputtering—the microscopic mechanisms and the variation of yield with experimental parameters.

Addressing the first objective is the most recent comprehensive compilation of experimental yield data for elemental targets, that of Matsunami *et al.*[2] They utilized all the published sputter yield measurements that were available in early 1983 (little has been published since that year), after screening the data according to criteria that increased its reliability. They published a collection of graphs showing yield as a function of energy, for normal incidence of the projectile.

In addition to the actual data points which they obtained from their literature search, they showed in each graph an empirical curve for the sputter yield as a function of projectile energy. The empirical curves are a means to compensate for the inaccuracies within even the screened experimental data. Matsunami *et al.* stated that ''*Agreement between the solid curve and the data points for each ion-target combination is generally satisfactory, ... the sputtering yield for any ion-target combination ... is accurate to within ±20% near the maximum of the sputtering yield while deviating somewhat more at lower and higher energies*.'' It should be added, though, that the actual experimental data itself is frequently not internally consistent to within ±20%. And for sputter deposition applications, the energy range well below the maximum (which occurs at typically a few tens of keV) is of primary interest.

One observes that in several of their graphs the empirical curve does not fit the experimental data at all. This may be surprising at first, since the empirical curves are described as ''best fits.'' The explanation is that a given curve was *not* obtained as a best-fit to the experimental yield data shown in the same graph. The curve is calculated using three empirical parameters in a formula that resembles Sigmund's high-energy yield expression.[3] The three parameters were determined as functions of m_t/m_p, the ratio of target to projectile mass. It is these three parameters which are best-fits—not to data for a specific projectile and target, but to practically all the available yield data, encompassing many projectile-target combinations.

The way the empirical curves were obtained, and the desire to generate them in the first place, raise the question of how to handle inconsistent sputtering data. Matsunami *et al.*'s empirical fitting procedure is based on the beliefs that the full set of data for all available projectile-target combinations is more reliable than any specific subset, and that the variations in yield between one combination of projectile, target, and energy, and a neighboring combination, are modest and smooth. Stated another way, yield data for elemental targets is believed to form a self-consistent, integrated, har-

 ©2000 The American Physical Society

monious whole such that the behavior of one elemental target can be inferred from that of its neighbors. Usage of the empirical curve implies that for a given projectile-target combination, the curve is more reliable than any actual data points. This reflects a skepticism toward the experimental data that has been widely held and which this present article supports.

To meet the second objective, understanding sputtering, data *trends are* revealing. Two trends of particular interest are the (1) *dependence of yield on target atomic number* for argon projectiles at, say, 1 keV (to make the data relevant to film deposition), and (2) *dependence of yield on the surface binding energy* of the target (again at 1 keV projectile energy).

The best-known and most widely referenced portrayal of the target dependence of sputter yield is probably the graph of Laegreid and Wehner showing the yield of 400-eV argon ions for twenty-eight pure element targets.[4] The way that the yield varies, as one moves across each row of the Periodic Table, has the same general form for each row. This observation of periodicity in yield led to a quest to find a single target parameter that is responsible. The result was summarized by Thompson: ''... *the well-known inverse dependence of yield on binding energy*.''[5] The weaknesses of this particular graph are that it is based solely on Laegreid and Wehner's 1961 data, and that the projectile energy is rather low (even for sputter deposition). Furthermore, the dependence of yield on surface binding energy will be shown in this article to be not strictly ''inverse.''

Another basic trend is (3) *the projectile-dependence of yield*. The best-known reference has been a graph by Almén and Bruce showing the yields of an incredible range of sixty-eight different 45-keV ions striking tantalum, copper, and silver targets.[6] Data for the inert gas projectiles in this graph are consistent with the widely held belief that ''*the heaviest inert gas will give the highest sputtering yield*.''[7] We will show in this article that for numerous widely used targets and a 1 keV projectile energy, the highest yield is *not* obtained with the heaviest inert gas projectile. The weaknesses of the Almén and Bruce reference (for present purposes) are that they utilized only their own 1961 data, and that the projectile energy is well above typical sputter deposition energies. Furthermore, because of the use of this rather high projectile energy the nonlinear cascade was very well developed in the copper and silver data (by all accepted measures).

To provide a bit of background, the linear cascade is believed to be the mechanism *mainly* responsible for sputtering in the film deposition regime. In a linear collision cascade, the number of recoils is sufficiently low that most collisions of the cascade involve one moving and one stationary particle. In the nonlinear cascade, on the other hand, the majority of atoms within the cascade volume are simultaneously in motion; when such a ''thermal spike'' occurs, the yield can be surprisingly high.

A second widely known example of the projectile dependence of yield is Andersen and Bay's data for silicon sputtered by twelve different projectiles.[8] The projectile energy was again 45 keV; this energy choice distorts the projectile mass dependence compared to that of a more typical film deposition energy. Thus, there is a need to update our understanding of these sputter yield trends with the best data available, for sputtering conditions typical of film deposition applications. (The three classic graphs just mentioned have been reproduced in a recent publication.[9])

The nonlinear cascade does occur in film deposition situations which are not exceptional, and another trend which we will identify in this paper is (4) *the transition to the nonlinear cascade*. This transition may be observed when comparing the 1-keV yield data of a wide variety of projectile-target combinations.

There is one final trend: (5) *the projectile energy-dependence of yield*. In the sputtering regime typical of film deposition (argon ions, common elemental targets, 0.5–2 keV projectile energy), the yield varies roughly as $E^{0.5}$. This behavior is in fact contained in Matsunami *et al.*'s empirical yield expression.

We will develop below the five data trends in some detail, and offer physical explanations for the behavior which are provided by a relatively new model of sputtering, the simplified collisional model.[9] In addition, we will lend some support to Matsunami *et al.*'s approach to the improvement of experimental yield data—combining the results of different experiments.

PROCEDURE

We obtained the experimental yield from Matsunami *et al.*'s graphs, at a projectile energy of 1 keV, for every combination of target and inert gas projectile available there. Our experimental yield values are those of the empirical curves, calculated with Matsunami *et al.*'s formula and parameters, not the experimental data points. In some instances the empirical curve at 1 keV projectile energy differs from the corresponding data point by more than 10%. Whenever this occurs we obtained a second estimate of yield, that of the actual experimental points themselves. Of the thirty one empirical yield values available for sputtering by argon, fourteen have divergent data points. (These divergent data points are shown in Fig. 1 only, to indicate the extent to which the empirical curves and the actual data do diverge.)

We also have calculated yield values using the simplified collisional model of sputter yield.[9] It has a closed-form yield expression, easily evaluated with a personal computer. To reiterate, in the following discussions, the empirical values will represent experiment, and the simplified collisional model values, theory. The few actual experimental data points shown in Fig. 1, which differ from the empirical curve values by more than 10%, will be called ''divergent data.'' We will make the case that the empirical curves are the best estimates of sputter yield that one has today; the model provides *understanding* of fundamental trends the data exhibit.

RESULTS

The target dependence of yield for 1-keV argon ion projectiles is shown in Fig. 1(a), where all of the available values from Matsunami *et al.*'s graphs are plotted. The divergent data points are more often above, rather than below, the empirical curve values. It is our belief that this particular divergence trend is due to the nonlinear cascade, which generates what has been termed an *excess* yield above that typi-

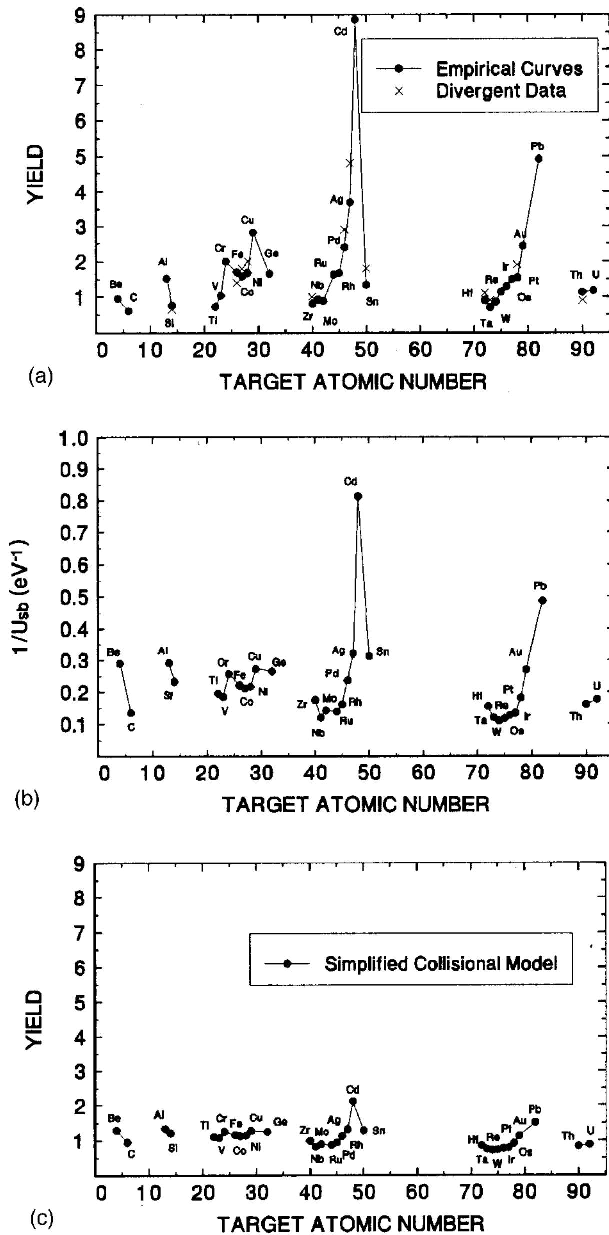

FIG. 1. (a) Experimental sputter yield of elemental targets by 1-keV argon projectiles, as a function of atomic number of the target. • represents yield values of the empirical curves of Matsunami *et al.* (Ref. 2) × represents yield values taken from the actual data points shown in the graphs of Matsunami *et al.*; this second yield estimate is added whenever the actual data differs from the empirical curve by 10% or more. (b) For the same elements as were shown in part (a), the reciprocal of surface binding energy (Refs. 13, 14) is plotted against atomic number. (c) Theoretical yield values of the simplified collisional model, for 1-keV argon projectiles, are plotted as a function of atomic number of the target. (Reprinted with permission from J. Mahan, *Physical Vapor Deposition of Thin Films*. Copyright 2000 by Wiley).

cal of, or even attributable to, the linear cascade sputtering mechanism.

For which projectile-target combinations does the nonlinear cascade occur at 1 keV? One must examine the yield data. As noted above, it produces yields which are in some sense ''excess.'' Thompson suggested that the critical yield for onset of the nonlinear cascade is about twenty.[5] Sigmund and Claussen put the value at ten,[10] while Zalm and Beckers suggested that the critical yield is seven.[11] We believe that the transition can be seen in Fig. 2, but before considering Fig. 2 in detail, we would like to explain its rationale.

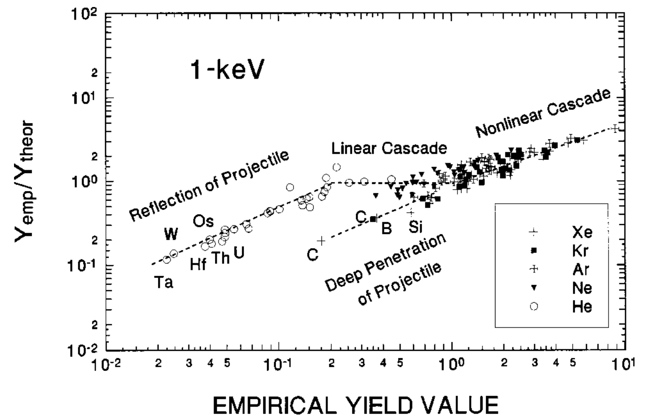

FIG. 2. Yield ratio (empirical/theoretical) at 1 keV plotted against empirical yield values for all combinations of noble gas projectiles and targets which are available in Matsunami *et al.* Four branches to the curve are identified. When the data is in the ''linear cascade'' regime and the assumptions of the simplified collisional model are valid, the yield ratio is constant. Excess yield due to the ''nonlinear cascade'' is apparent for empirical yield values above ~1. Sometimes the data is in the linear cascade regime but the assumptions of the simplified collisional model are *not* valid. These branches are ''reflection of projectile'' and ''deep penetration of projectile.''

We believe that the transition to the nonlinear cascade may be discerned by observing the correlation between Matsunami *et al.*'s empirical yields and the theoretical yields of a linear cascade model, for various projectile-target combinations. Some of these experimental yields will be in the linear cascade regime, and some experimental yields will be the result of nonlinear cascade sputtering. We expect a rough proportionality between Y_{emp} and Y_{theor} when in the linear cascade regime, and a superlinear departure from proportionality will signal the onset of the nonlinear cascade. It doesn't matter if $Y_{\mathrm{emp}} \neq Y_{\mathrm{theor}}$ in the linear cascade regime (the proportionality constant might not be 1.0); what this argument depends upon is that $Y_{\mathrm{emp}} \propto Y_{\mathrm{theor}}$ when the sputtering mechanism is the linear cascade for both experiment and theory. In Fig. 2 the simplified collisional model has been used to provide the theoretical linear cascade yields. This model is indeed a linear one: the number of recoils is proportional to the projectile's energy, and the theoretical yield is proportional to the energy deposited in a thin surface layer of the target. And as just stated, its absolute accuracy need not be assumed for the purpose of this argument.

For all the targets and inert gas projectiles available in the Matsunami *et al.* graphs, we show in Fig. 2 the ratio $Y_{\mathrm{emp}}/Y_{\mathrm{theor}}$ plotted against the empirical yield values. The original purpose in constructing this plot was to find the onset of the nonlinear cascade, but the plot contains much more information than this. It is possible to identify four distinct branches in this plot, which are indicated with dashed lines placed by eye, and we provide the following interpretation. The four branches are distinguished by four physical effects. First, there is a horizontal branch in the

center, for yields of ~0.2 to ~1.0, where $Y_{emp} \propto Y_{theor}$ (and in fact $Y_{emp} \approx Y_{theor}$). Experiment is indeed in the linear cascade regime, and the assumptions of the simplified collisional model are valid. In the branch on the right side of the figure, the yield ratio begins to climb at a critical yield of ~1, which represents the onset of the nonlinear cascade mechanism. This Y_{emp} estimate is not very accurate, but the point of departure from proportionality in Fig. 2, wherever one places it, is clearly lower than the critical yield values quoted above (20, 10, and 7). This may be because the definition of Y_{crit} has been unclear—is it the yield for which excess yield *equals* linear cascade yield, or perhaps *dominates* the yield value? We take it to mean the value at which the empirical yield *first deviates detectably* from a linear cascade value.

The third and fourth branches are regimes where the experimental mechanism is the linear cascade, but assumptions of the simplified collisional model are invalid. The third branch contains the lowest yields in the figure. We hypothesize that here, backscattering of the projectile occurs to a significant degree, allowing the projectile to escape from the target before depositing all of its energy. The data points which make up this branch are, as one might expect, the sputtering of heavy targets by the lightest of all projectiles, helium. In TRIM simulations of the helium sputtering of tungsten which we ran for the purpose of checking this idea, approximately one third of the projectiles were backscattered. Now, backscattering is not recognized by the model. Consequently, the model overestimates the yield for these projectile-target combinations. While sputtering with helium is not relevant to thin-film deposition, this data is valuable for understanding the mechanisms of sputtering.

Finally, the fourth branch is in the center of the figure but below the linear cascade branch. Here, the model again overestimates the yield, but for a different reason: There is particularly deep penetration of the projectile. In this case the recoils probably do not have the isotropic velocity distribution assumed by the model, but rather one that is directed into the target. Thus, the probability of escape of the recoils is lower than that assumed in the model. As one might expect, the data points making up this branch are rather light targets sputtered by the heaviest projectiles, krypton and xenon.

We draw three conclusions from this analysis. (1) Excess yield due to the nonlinear cascade is detectable for yield values exceeding ~1. (2) There is good (in sputtering, agreement to within a factor of 2 is often considered ''good'') correspondence between theory and experiment for yields below 1, except when there is a large difference between projectile and target masses. (3) It could well be true that the nonlinear cascade is the main sputtering mechanism in thin film deposition situations, since many data points in Fig. 2 seem to be in that regime. It appears that there is a need for a nonlinear cascade sputtering model which is useful to the nonspecialist (i.e., another ''simplified'' model[9]).

Returning to the target-dependence of yield in Fig. 1(a) the rows of the Periodic Table are represented as follows:

Be→C represent the second row,

Al→Si represent the third,

Ti→Ge the fourth,

Zr→Sn the fifth,

Hf→Au the sixth, and

Th→U the actinide series.

One searches here for the expected variation in yield that repeats with each row of the Periodic Table. If it is there, it is not terribly strong in this, today's best available summary of the target-dependence of yield by 1-keV argon projectiles. On might generalize, at least, that there is an uptick when one hits a noble metal and there is a drop when one arrives at a Column IVB element (ignoring lead). On the other hand, viewing the empirical yields simply as a function of target atomic number, some other target parameter must be more fundamental.

What is the single most important target parameter—the one to which the yield is most sensitive—and is there one for which the yield varies monotonically? The simplified collisional model suggests that the one previously identified by Thompson[5] and others,[12] surface binding energy, is the only possible choice. In that model there are four target parameters that enter the yield calculation: atomic number, atomic mass, surface binding energy, and atomic density. A plot of yield versus target atomic mass is very similar to the atomic number plot. Plots of yield versus target density (both empirical and theoretical, neither of which are shown) revealed no systematic dependence of yield on this parameter. Indeed, in the simplified collisional model the final yield expression is independent of target density (although it enters into the calculation of projectile and recoil ranges). Thus, we pursue the historical choice, the surface binding energy, as the single most important target parameter.

We are not the first to show that the yield is *roughly* a monotonic function of U_{sb}. Following Carter and Colligon, who produced the first version of this plot in 1968,[12] we show in Fig. 1(b) the reciprocals of the surface binding energy values as a function of atomic number of the target.[13,14] The similarity between Figs. 1(a) and 1(b) is striking. One is tempted to develop an empirical yield expression simply of the form $Y \sim \mathrm{const}/U_{sb}$. However, we will shown next that the dependence of Y on U_{sb} is not strictly reciprocal, and it is already clear that other target parameters besides U_{sb} (atomic number and mass) play a significant role.

Insight into the functional dependence of Y on U_{sb}, and the strength of the dependence, may be obtained with the empirical and theoretical data plotted in Fig. 3. In order to do some quantitative analysis, we assumed that

$$Y(U_{sb}) = \frac{A}{(U_{sb})^n}, \tag{1}$$

and determined the best values of the constants (A and n) by nonlinear regression analysis. If *all* the empirical data points in Fig. 3(a) are used, the best-fit exponent is actually 1.31. This rather high value cannot be representative of linear cascade sputtering, because there is some excess yield due to the nonlinear cascade whenever the yield exceeds the critical value of ~1.

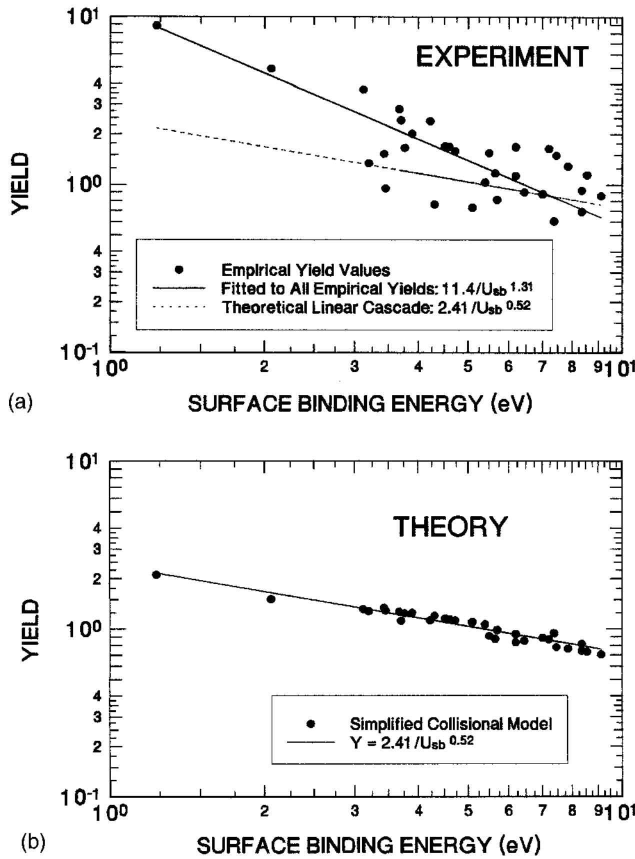

FIG. 3. (a) Empirical yield values for 1-keV argon projectiles are plotted versus surface binding energy. All the targets of Fig. 1 are shown. The solid line shows the function, $A/(U_{sb})^n$, which was fitted to the empirical values by nonlinear regression analysis. The dashed line is the fit to theoretical yields obtained in part b. (b) Theoretical yield values, calculated with the simplified collisional model, are plotted versus surface binding energy. (Reprinted with permission from J. Mahan, *Physical Vapor Deposition of Thin Films*. Copyright 2000 by Wiley.)

The pure linear cascade, as represented by the simplified collisional model, is analyzed in Fig. 3(b). We plot there the theoretical yields for all the targets, against surface binding energy. Assuming again a functional dependence in the form of Eq. (1) the exponent was found to be 0.52. [For reference, a dashed line having these coefficients is also plotted in Fig. 3(a)]. We generalize that for the linear cascade, $Y \propto U_{sb}^{-0.5}$ as a rule of thumb. The stronger U_{sb} dependence occurs only when mixed data-linear and nonlinear cascade-are combined.

The actual yield expression of the simplified collisional model is[15]

$$Y = \frac{E}{E_{\mathrm{ave}}} \cdot \frac{R^{p}_{r,\mathrm{eff}}}{R^{p}_{p}} \cdot 1/4, \tag{2}$$

where E is the projectile energy, E_{ave} is the average energy of the recoils at termination of the collision cascade, $R^{p}_{r,\mathrm{eff}}$ is the effective projected range of a target recoil, and R^{p}_{p} is the projected range of a projectile. The first ratio (energy) gives the effective number of recoils that are created by a single projectile. The other two ratios give the fraction of those recoils that are close enough to the surface to escape (the range ratio) and that are traveling in the right direction (1/4). The point here is that the hidden functional dependence of yield on surface binding energy in this theoretical expression is quite complex, but to a large degree it is contained within $1/E_{\mathrm{ave}}$, where

$$\frac{1}{E_{\mathrm{ave}}} = \frac{1}{[U_{sb} ln[\gamma E/U_{sb}]}. \tag{3}$$

γ is the energy transfer mass factor of binary collision theory, $4m_p m_t/(m_p+m_t)^2$. m_p and m_t are the projectile and target masses.[9] If theoretical $\log E_{\mathrm{ave}}$ values are plotted versus $\log U_{sb}$, and analyzed with linear regression, one finds a good fit with $E_{\mathrm{ave}} = 7.47 U_{sb}{}^{0.5}$ (with both energies expressed in eV).

One observes in Fig. 3 that the scatter in the empirical yield values is much greater than that of the theoretical yields of the simplified collisional model. Indeed, in the nonlinear regression analysis of the empirical $Y(U_{sb})$ values the standard deviation from the best-fit function is 0.56, while for the theoretical values it is only 0.06. The theoretical plot gives one the quantitative perspective to say that there is a lot of scatter in the empirical data. (We are ignoring here any possible error in the U_{sb} values, because they originate with the relatively refined thermochemical data.)

What are the sources of scatter in Fig. 3(a)? Experimental error is surely present, but if the yield is a function of several target parameters and is plotted as a function of U_{sb} only, then there will be scatter in the yield values even in the absence of experimental error. Thus, there should be some *intrinsic* scatter in yield data plotted as a function of U_{sb}, which could not be removed even with perfect experimentation.

How can this intrinsic scatter be estimated? The simplified collisional model contains *all* target properties which are likely to be significant (surface binding energy, atomic mass and number, and density). If one accepts this model, then the theoretical plot [Fig. 3(b)] may be thought of as portraying the U_{sb} dependence of yield for the linear cascade sputtering mechanism with *no* experimental error (assuming that the surface binding energy values are correct). Using the above-mentioned standard deviation of 0.06, the average deviation of theoretical $Y(U_{sb})$ from the best-fit line is $10^{0.06}$, or $\sim$1.15. The intrinsic scatter, then, is estimated to be $\pm$15%.

We suspect that the scatter among the empirical points of Fig. 3(a) originates largely with experimental error. Their standard deviation from their best-fit line is 0.56 (as mentioned above). Thus, the average deviation of empirical $Y(U_{sb})$ from the best-fit line is $10^{0.56}$, or a factor of 3.63. The averaging approach behind Matsunami's empirical curves seems justified.

Figure 1(c) shows the theoretical yields as a function of target atomic number, drawn using the same scale as in Fig. 1(a). The large yields of the nonlinear cascade are absent, and again, there is less scatter among the theoretical yield values than in the empirical data [cf. Fig. 1(a)].

Moving now to the next trend, the general behavior for projectile dependence of yield (as well as target dependence) at 1 keV is shown in Fig. 4. This is a qualitative contour plot representing empirical yield values as a function of both projectile atomic number and target atomic number. The $\sim$90 discrete data points underlying this plot have been smoothed

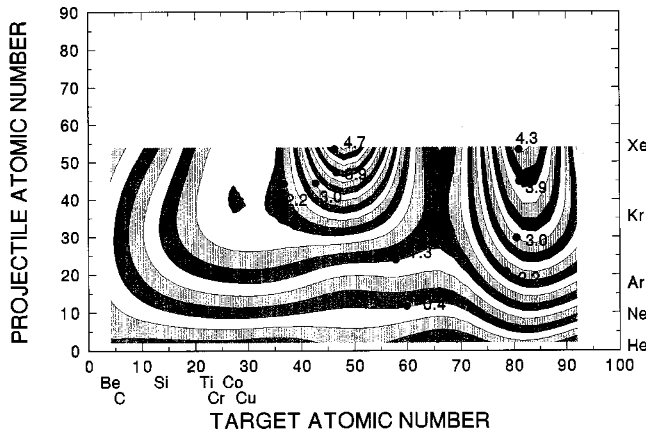

FIG. 4. This contour plot suggests the variations of empirical sputter yield with both projectile and target atomic number. All the targets that exhibit intermediate maxima as a function of projectile atomic number are specifically listed; the rest exhibit terminal maxima at xenon. (Reprinted with permission from J. Mahan, *Physical Vapor Deposition of Thin Films*. Copyright 2000 by Wiley.)

and fitted with a three-dimensional surface. We used all the available cases for 1-keV inert gas projectiles from Matsunami *et al.*'s compilation. (The generous axis ranges were chosen to allow direct comparison to a later theoretical plot.) *The yield increases monotonically with projectile mass only for the heavier targets. For the lighter targets the yield exhibits a maximum at an intermediate projectile mass*, usually krypton. (The seven targets that exhibit an intermediate maximum in empirical yield as a function of projectile mass are identified specifically in the figure.)

As a detailed example of the difference in behavior between heavy and light targets, we show in Fig. 5(a) the empirical yield as a function of projectile atomic number for Column IVB elements. The yield peaks with the argon ion for a silicon target, and most probably with either neon or argon for a carbon target (missing data prevents one from saying which projectile). On the other hand, for the two heaviest elements shown, germanium and tin (empirical lead data was not available), the yield rises monotonically all the way to xenon.

These same projectile dependence trends are exhibited by the calculated yields of the simplified collisional model. As shown in Fig. 5(b), the yield curves exhibit maxima for carbon, silicon, and germanium. The maximum in yield for carbon and silicon occurs for the krypton projectile (in modest disagreement with the carbon and silicon data, which have an intermediate maximum but not at krypton), while for germanium the maximum occurs for xenon. For tin and lead, the yield increases all the way to radon.

What is the physical basis of these trends with projectile mass? The yield expression of the simplified collisional model offers some insight. We will compare the two extreme behaviors, those of carbon and lead. First, the explanation does not rest with the E/E_{ave} term itself: For carbon, our calculations show that E_{ave} exhibits a slight maximum at neon while for lead, E_{ave} increases monotonically with projectile mass; considering the yield expression in Eq. (2) ($Y \propto 1/E_{\mathrm{ave}}$), these run counter to the trends. The explanation lies with the ratio of projected ranges, $R^p_{r,\mathrm{eff}}/R^p_p$. For carbon

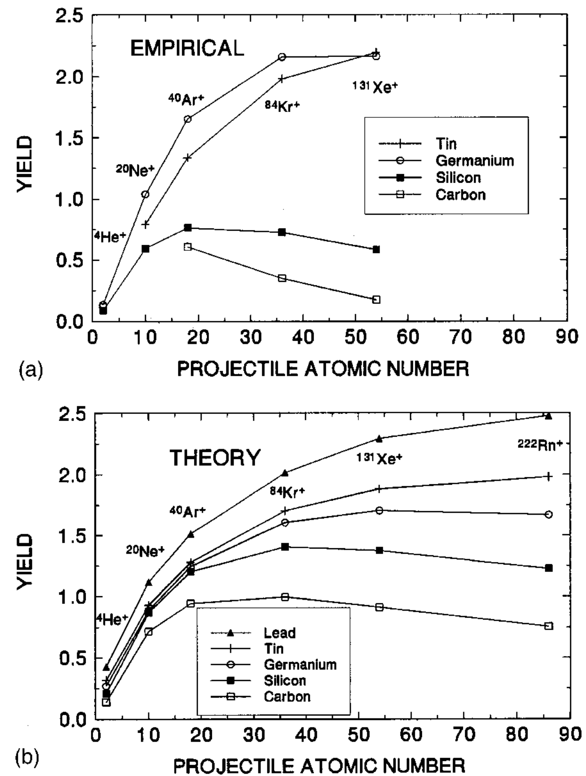

FIG. 5. (a) Empirical yield values for Column IVB elements of the Periodic Table are plotted as a function of projectile atomic number. The projectile energy is 1 keV. (b) Theoretical yield values for Column IVB elements are plotted as a function of projectile atomic number. The projectile energy is again 1 keV. (Reprinted with permission from J. Mahan, *Physical Vapor Deposition of Thin Films*. Copyright 2000 by Wiley.)

the ratio as calculated theoretically exhibits an intermediate maximum at argon; the projectile dependence of the E/E_{ave} term shifts the overall maximum in yield to krypton. For lead the range ratio increases monotonically with projectile mass; this accounts for lead's yield trend.

But why, physically, does the range ratio depend on projectile mass as it does? The behavior is primarily due to R^p_p. R^p_p is inversely proportional to the nuclear energy loss cross-section, which peaks when the projectile and target masses are equal. Thus, R^p_p for a heavy target falls continually with increasing projectile mass while for a light target, R^p_p exhibits an intermediate minimum. R^p_p by itself qualitatively rationalizes all the projectile-dependence trends as described in the preceding paragraph.

$R^p_{r,\mathrm{eff}}$ also plays a role, varying in a way that further supports the trend, but its dependence on projectile mass is indirect and thus harder to understand. For carbon $R^p_{r,\mathrm{eff}}$ exhibits a maximum at neon (because E_{ave} does—in the model $R^p_{r,\mathrm{eff}}$ is proportional to E_{ave}) while for lead, $R^p_{r,\mathrm{eff}}$ increases monotonically with projectile mass (again, because E_{ave} does); these dependences are consistent with the intermediate maximum in yield for carbon and the monotonic increase in yield for lead. To summarize, the projectile-dependence of the ratio $R^p_{r,\mathrm{eff}}/R^p_p$ accounts for the projectile dependence of calculated yield and this behavior may be understood as arising primarily with the projected range of the projectile.

The simplified collisional model predicts that several

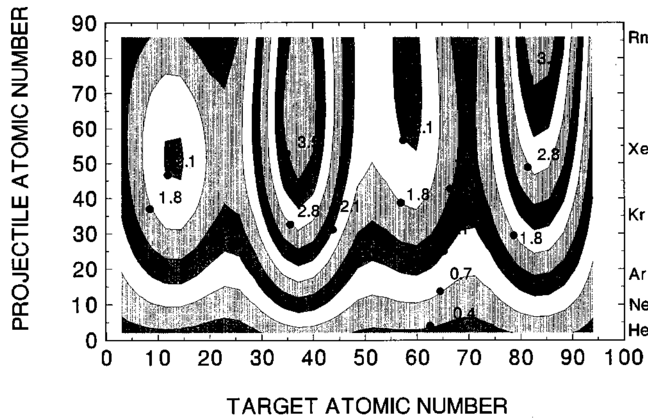

FIG. 6. This contour plot suggests the variations of theoretical sputter yield with both projectile and target atomic number. The heaviest inert gas, radon, has been added (no experimental yield data was available). As a result, the number of targets which exhibit intermediate maxima as a function of projectile atomic number is increased (compared to Fig. 4). (Reprinted with permission from J. Mahan, *Physical Vapor Deposition of Thin Films*. Copyright 2000 by Wiley.)

other target materials will exhibit intermediate maxima in yield as a function of projectile mass, if the heaviest inert gas, radon, is included (no radon sputtering data is found in Matsunami *et al.*). This is shown in the contour plot of theoretical 1 keV yields in Fig. 6 (again, a surface fitted to the data and smoothed). Yields were calculated for every element of the Periodic Table for which surface binding energy and density are known; 462 projectile-target combinations are represented. The model predicts that all the elements of atomic number 34 and below exhibit intermediate maxima in yield versus projectile atomic number. For the lightest targets, the yield maximum actually occurs for krypton, while for slightly heavier targets the maximum in yield occurs with xenon. For target atomic numbers above 34, there is a terminal maximum at radon.

Figure 7 shows the calculated 1 keV yields for all 462 projectile-target combinations. As with Fig. 6, this plot includes cases (all of the radon projectile yields, plus some

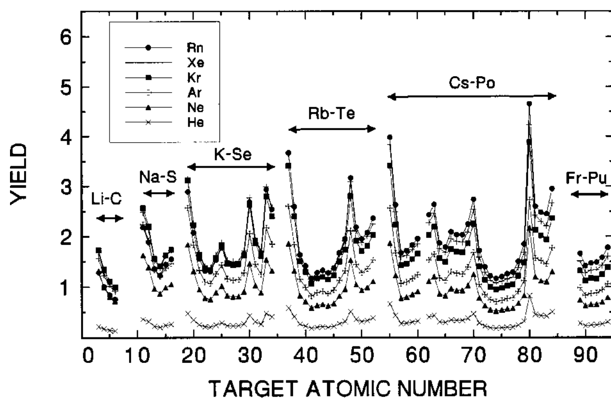

FIG. 7. Theoretical sputter yields as a function of target atomic number are shown, for all the inert gas projectiles. The extent of representation of each row of the Periodic Table is shown with arrows. (Reprinted with permission from J. Mahan, *Physical Vapor Deposition of Thin Films*. Copyright 2000 by Wiley.)

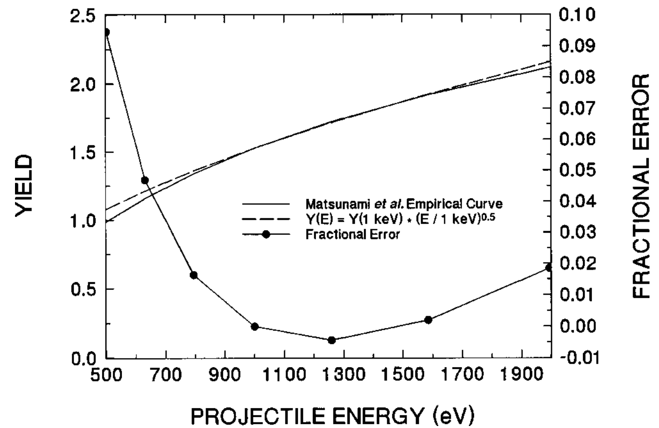

FIG. 8. Sputter yield of aluminum as a function of argon projectile energy. Both the empirical curve of Matsunami *et al.* and the approximation to it given in the text are shown. The fractional error is less than 10% over the energy range shown.

others besides) for which no empirical data is available. One can finally see here a periodicity that was not entirely clear in Fig. 1, where the yield behavior repeats for each row of the Periodic Table (the extent of each row is marked with arrows). The variation across a row is V or W shaped. Furthermore, the choice-of-projectile trend is clearly discernable in these purely linear cascade yields. Radon gives the highest yields only for the heaviest targets. Xenon has the highest yields for targets of intermediate mass, while krypton gives the highest yields for the lightest targets. The most widely used sputtering gas, argon, never gives the highest yield.

All of the theoretical 1 keV yields of Fig. 7 are tabulated in the Appendix for reference purposes in film deposition applications. In addition, the 1-keV empirical yield values of Matsunami *et al.* are tabulated in this Appendix, for all six inert gas projectiles and for all targets for which empirical parameters are available.

The empirical yield for a given projectile-target combination, but at another energy between ~0.5 and ~2 keV, may be estimated from

$$Y(E) \approx Y(1\,\text{keV}) \cdot (E/1\,\text{keV})^{0.5}. \tag{4}$$

This is an approximation to Matsunami *et al.*'s empirical function which is valid when the projectile energy is much greater than the threshold energy, and when the reduced projectile energy[9] is much less than one (usually true for argon but not always so for the heavier inert gases). As a practical example, we show in Fig. 8 the yield of aluminum as a function of argon projectile energy. Curves calculated with both the empirical formula of Matsunami *et al.* and the above approximation are shown. The fractional error is under 10% throughout the energy range stated above. This energy dependence is identical to that of a more complete semi-empirical formula developed by Steinbrüchel.[16]

As we have just seen, both the simplified collisional model and Matsunami *et al.*'s empirical formula provide predictions of yield in cases where no actual experimental data is available. We have included in the Appendix some empirical yield values that were calculated using Matsunami *et al.*'s empirical formula and that are not represented by any actual experimental data in Matsunami *et al.*'s graphs. It is

straightforward to use their empirical expressions and parameter values to do this. These cases include the sputter yields of all targets by radon projectiles, plus the yields of numerous targets sputtered by helium, neon, argon, krypton, and xenon. (In the body of this article, these projectile-target combinations that are without actual experimental representation play no part in the discussions.)

SUMMARY AND CONCLUSIONS

We would like to suggest the following statements as summarizing five trends in sputter yield data:
(1) There is a periodicity in yield values when plotted against target atomic number, repeating across each row of the Periodic Table.
(2) Surface binding energy is the most important target parameter in determining the variation in sputter yield from one target to another. For empirical data at 1 keV the functional dependence is approximately

$$Y \propto 1/U_{sb}^{1.3},$$

while for the pure linear cascade sputtering mechanism,

$$Y \propto 1/U_{sb}^{0.5}.$$

(3) Excess yield due to the nonlinear cascade becomes discernable when the yield exceeds ~1.
(4) For target atomic numbers above ~34, the 1 keV yield increases monotonically with inert gas projectile mass; for lighter targets the yield exhibits a maximum at an intermediate projectile mass.
(5) The energy dependence of yield for fixed projectile-target combinations from 0.5 to 2 keV may be estimated from

$$Y(E) \propto Y(1\ \mathrm{keV}) \cdot (E/1\ \mathrm{keV})^{0.5}.$$

As a general rule, the empirical sputter yield data exhibit much more scatter than theoretical yields, due to experimental error. Consequently, some averaging or smoothing of the results, such as the creation of Matsunami's empirical curves, is called for. The idea that combined experiments give a more reliable result than a single experiment standing alone is well established.[17]

What insight, then, do data and model each provide? For quantitative estimates of yield values we recommend employing the empirical curves of Matsunami *et al.* Good judgment requires considering any divergent data. For interpretation of the data and understanding the mechanisms of sputtering, the simplified collisional model offers insight. In addition, both the simplified collisional model and the empirical formula provide yield estimates for cases where there is no available experimental data.

ACKNOWLEDGMENT

A.V. received financial support from the Fund for Scientific Research, Flanders, Belgium.

APPENDIX: SPUTTER YIELD VALUES AT 1 keV

For each projectile-target combination, Matsunami *et al.*'s empirical yield value is followed by the theoretical yield value of the simplified collisional model, √ indicates an empirical yield value that is represented by actual experimental data in Matsunami *et al.*'s graphs. M stands for a missing value, either empirical or theoretical (one for which we could not obtain all the necessary data to calculate a yield value).

PROJECTILE

TARGET	Helium		Neon		Argon		Krypton		Xenon		Radon	
	Emp.	Theor.	Emp.	Theor.	Emp.	Theor.	Emp.	Theor.	Empt.	Theor.	Emp.	Theor.
Lithium	M	0.2143	M	1.3139	M	1.6903	M	1.7336	M	1.5656	M	1.2822
Beryllium	0.1870√	0.1712	0.974√	0.9904	0.953√	1.2904	0.645√	1.3442	0.402√	1.2228	0.165	1.0067
Boron	0.2150	0.1464	1.176	0.8035	1.118	1.0546	0.680	1.1101	0.368	1.0150	0.104	0.8380
Carbon	0.1160	0.1377	0.645	0.7185	0.606√	0.9429	0.350√	0.9960	0.176√	0.9130	0.040	0.7555
	M	M	M	M	M	M	M	M	M	M	M	M
	M	M	M	M	M	M	M	M	M	M	M	M
	M	M	M	M	M	M	M	M	M	M	M	M
	M	M	M	M	M	M	M	M	M	M	M	M
Sodium	M	0.3615	M	1.6245	M	2.2377	M	2.5654	M	2.4775	M	2.1778
Magnesium	M	0.3165	M	1.3887	M	1.9131	M	2.2031	M	2.1346	M	1.8839
Aluminum	0.1890√	0.2245	1.179√	0.9641	1.526√	1.3365	1.491√	1.5597	1.231√	1.5232	0.820	1.3544
Silicon	0.0893√	0.2061	0.591√	0.8682	0.762√	1.2026	0.726√	1.4067	0.581√	1.3770	0.365	1.2276
Phosphorus	M	0.2388	M	0.9854	M	1.3724	M	1.6261	M	1.6055	M	1.4445
Sulfur	M	0.2589	M	1.0498	M	1.4607	M	1.7352	M	1.7172	M	1.5496
	M	M	M	M	M	M	M	M	M	M	M	M
	M	M	M	M	M	M	M	M	M	M	M	M
Potassium	M	0.4750	M	1.8362	M	2.5727	M	3.1257	M	3.1446	M	2.8902
Calcium	M	0.3442	M	1.3097	M	1.8321	M	2.2311	M	2.2482	M	2.0713
Scandium	M	0.2520	M	0.9431	M	1.3258	M	1.6394	M	1.6703	M	1.5566
Titanium	0.0648√	0.2111	0.497√	0.7803	0.731√	1.0987	0.831√	1.3676	0.751√	1.4013	0.555	1.3139
Vanadium	0.0860√	0.2071	0.693√	0.7554	1.034√	1.0651	1.191√	1.3348	1.082√	1.3750	0.802	1.2973

	PROJECTILE											
TARGET	Helium		Neon		Argon		Krypton		Xenon		Radon	
Chromium	0.1830√	0.2468	1.342√	0.8885	2.009√	1.2505	2.372√	1.5691	2.210√	1.6196	1.715	1.5317
Manganese	0.2824√	0.2857	1.887	1.0161	2.859	1.4302	3.496√	1.8046	3.365√	1.8724	2.752	1.7813
Iron	0.1500√	0.2335	1.122√	0.8232	1.704√	1.1575	2.050√	1.4616	1.934√	1.5185	1.522	1.4460
Cobalt	0.1350√	0.2299	1.032√	0.8023	1.584√	1.1278	1.934√	1.4320	1.841√	1.4944	1.465	1.4318
Nickel	0.1450√	0.2351	1.098√	0.8138	1.682√	1.1421	2.048√	1.4469	1.947√	1.5097	1.545	1.4467
Copper	0.2540√	0.2655	1.815√	0.9055	2.822√	1.2731	3.563√	1.6260	3.493√	1.7080	2.909	1.6508
Zinc	0.7599	0.4325	4.287	1.4597	6.679	2.0509	8.785	2.6280	8.993	2.7658	8.067	2.6852
Gallium	M	0.3076	M	1.0274	M	1.4446	M	1.8580	M	1.9672	M	1.9210
Germanium	0.1370√	0.2676	1.038√	0.8865	1.654√	1.2442	2.160√	1.6088	2.164√	1.7096	1.847	1.6748
Arsenic	M	0.4714	M	1.5403	M	2.1669	M	2.7990	M	2.9870	M	2.9367
Selenium	M	0.4060	M	1.3150	M	1.8436	M	2.3988	M	2.5692	M	2.5378
	M	M	M	M	M	M	M	M	M	M	M	M
	M	M	M	M	M	M	M	M	M	M	M	M
Rubidium	M	0.5860	M	1.8540	M	2.5977	M	3.4133	M	3.6523	M	3.6693
Strontium	M	0.4150	M	1.3135	M	1.8311	M	2.3986	M	2.5844	M	2.5914
Yttrium	M	0.2617	M	0.8237	M	1.1477	M	1.5043	M	1.6257	M	1.6308
Zirconium	0.0485√	0.2255	0.483√	0.7089	0.811√	0.9869	1.108√	1.2932	1.133√	1.4026	0.979	1.4117
Niobium	0.0486√	0.1844	0.544√	0.5838	0.924√	0.8130	1.260√	1.0668	1.280√	1.1572	1.086	1.1661
Molybdenum	0.0487√	0.2033	0.518√	0.6359	0.879√	0.8852	1.215√	1.1643	1.251√	1.2653	1.085	1.2801
Technetium	M	0.2109	M	0.6530	M	0.9086	M	1.1951	M	1.3027	M	1.3220
Ruthenium	0.0888	0.2015	0.954√	0.6244	1.633√	0.8660	2.291√	1.1428	2.388√	1.2476	2.108	1.2712
Rhodium	0.1010√	0.2192	0.983√	0.6718	1.674√	0.9312	2.370√	1.2291	2.499√	1.3453	2.254	1.3700
Palladium	0.1770√	0.2707	1.420√	0.8138	2.390√	1.1270	3.441√	1.4932	3.713√	1.6369	3.488	1.6734
Silver	0.3110√	0.3163	2.209√	0.9514	3.688√	1.3152	5.354√	1.7341	5.843√	1.9039	5.604	1.9489
Cadmium	1.0082	0.5139	5.386	1.5277	8.862√	2.1058	13.137	2.8024	14.738	3.0903	14.828	3.1652
Indium	M	0.3539	M	1.0471	M	1.4405	M	1.9087	M	2.1101	M	2.1809
Tin	0.1068	0.3156	0.791√	0.9285	1.337√	1.2797	1.981√	1.7042	2.195√	1.8811	2.145	1.9481
Antimony	M	0.3367	M	0.9857	M	1.3573	M	1.8093	M	2.0007	M	2.0735
Tellurium	M	0.3816	M	1.1055	M	1.5243	M	2.0298	M	2.2515	M	2.3582
Iodine	M	M	M	M	M	M	M	M	M	M	M	M
	M	M	M	M	M	M	M	M	M	M	M	M
Cesium	M	0.6607	M	1.8645	M	2.5611	M	3.4163	M	3.8303	M	3.9819
Barium	M	0.4308	M	1.2211	M	1.6656	M	2.2340	M	2.4881	M	2.6243
Lanthanum	M	0.2713	M	0.7778	M	1.0665	M	1.4254	M	1.5913	M	1.6702
Cerium	M	0.2791	M	0.7972	M	1.0908	M	1.4515	M	1.6206	M	1.7142
Praeseodynium	M	0.3013	M	0.8479	M	1.1581	M	1.5466	M	1.7358	M	1.8296
Neodymium	M	0.3224	M	0.9050	M	1.2376	M	1.6525	M	1.8419	M	1.9507
Promethium	M	M	M	M	M	M	M	M	M	M	M	M
Samarium	M	0.4036	M	1.1128	M	1.5234	M	2.0230	M	2.2705	M	2.4301
Europium	M	0.4330	M	1.2029	M	1.6447	M	2.1898	M	2.4543	M	2.6377
Gadolinium	M	0.3090	M	0.8598	M	1.1680	M	1.5636	M	1.7555	M	1.8683
Terbium	M	0.2972	M	0.8211	M	1.1201	M	1.4918	M	1.6778	M	1.7886
Dysprosium	M	0.3455	M	0.9606	M	1.2961	M	1.7439	M	1.9531	M	2.0890
Holmium	M	0.3359	M	0.9257	M	1.2663	M	1.6877	M	1.8934	M	2.0295
Erbium	M	0.3361	M	0.9273	M	1.2488	M	1.6823	M	1.8883	M	2.0284
Thulium	M	0.3769	M	1.0225	M	1.3844	M	1.8646	M	2.0834	M	2.2416
Ytterbium	M	0.4609	M	1.2411	M	1.6797	M	2.2499	M	2.5372	M	2.7388
Lutetium	M	0.2844	M	0.7745	M	1.0436	M	1.4011	M	1.5865	M	1.7153
Hafnium	0.0374√	0.2246	0.487√	0.6266	0.901√	0.8484	1.452√	1.1339	1.696√	1.2857	1.759	1.3945
Tantalum	0.0224√	0.1913	0.363√	0.5468	0.691√	0.7393	1.121√	0.9942	1.306√	1.1208	1.339	1.2183
Tungsten	0.0246√	0.1800	0.443√	0.5213	0.856√	0.7053	1.398√	0.9483	1.629√	1.0722	1.666	1.1620
Rhenium	0.0366	0.1882	0.597√	0.5388	1.139√	0.7298	1.860√	0.9737	2.178√	1.1060	2.251	1.2001
Osmium	0.0397√	0.1972	0.670√	0.5617	1.285√	0.7615	2.109√	1.0199	2.478√	1.1570	2.574	1.2585
Iridium	0.0548√	0.2054	0.793√	0.5759	1.492√	0.7787	2.445√	1.0445	2.889√	1.1833	3.040	1.2883
Platinum	0.0668√	0.2465	0.834√	0.6723	1.542√	0.9077	2.524√	1.2165	3.001√	1.3780	3.199	1.4997

TARGET	PROJECTILE Helium		Neon		Argon		Krypton		Xenon		Radon	
Gold	0.1510√	0.3115	1.365√	0.8227	2.429√	1.1181	3.951√	1.4818	4.739√	1.6797	5.161	1.8470
Mercury	M	0.8202	M	2.1659	M	2.7315	M	3.8856	M	4.2279	M	4.6535
Thallium	M	0.4514	M	1.1908	M	1.5615	M	2.1252	M	2.4131	M	2.5984
Lead	0.4470√	0.4272	2.861	1.1149	4.911√	1.5133	7.993	2.0144	M	2.2932	10.915	2.4768
Bismuth	M	0.4189	M	1.0971	M	1.4510	M	1.9371	M	2.2086	M	2.4466
Polonium	M	0.5030	M	1.2993	M	1.7670	M	2.3600	M	2.6615	M	2.9482
Astatine	M	M	M	M	M	M	M	M	M	M	M	M
	M	M	M	M	M	M	M	M	M	M	M	M
Francium	M	M	M	M	M	M	M	M	M	M	M	M
Radium	M	M	M	M	M	M	M	M	M	M	M	M
Actinium	M	0.2787	M	0.7397	M	0.9774	M	1.3149	M	1.5028	M	1.6596
Thorium	0.0408√	0.2276	0.594√	0.6248	1.126√	0.8305	1.904√	1.1145	2.326√	1.2706	2.577	1.4126
Protactinium	M	0.2417	M	0.6496	M	0.8643	M	1.1643	M	1.3216	M	1.4672
Uranium	0.0469√	0.2463	0.624√	0.6583	1.169√	0.8726	1.977√	1.1556	2.427√	1.3312	2.718	1.4819
Neptunium	M	0.2643	M	0.6987	M	0.9378	M	1.2402	M	1.4212	M	1.5780
Plutonium	M	0.3013	M	0.7872	M	1.0480	M	1.3800	M	1.6024	M	1.7777

[1] For numerous examples, consider the plots of H. H. Andersen and H. L. Bay, in *Sputtering by Particle Bombardment I*, edited by R. Behrish (Springer-Verlag, Berlin, 1981).

[2] N. Matsunami, Y. Yamamura, Y. Itikawa, N. Itoh, Y. Kazumata, S. Miyagawa, K. Morita, R. Shimizu, and H. Tawara, At. Data Nucl. Data Tables **31**, 1 (1984).

[3] P. Sigmund, Phys. Rev. **184**, 383 (1969).

[4] N. Laegreid and G. K. Wehner, J. Appl. Phys. **32**, 365 (1961).

[5] M. W. Thompson, Phys. Rep. **69**, 335 (1981).

[6] O. Almén and G. Bruce, Nucl. Instrum. Methods **11**, 279 (1961).

[7] B. Chapman, *Glow Discharge Processes* (Wiley-Interscience; New York, 1980).

[8] H. H. Andersen and H. L. Bay, J. Appl. Phys. **46**, 1919 (1975).

[9] J. E. Mahan and A. Vantomme, J. Vac. Sci. Technol. A **15**, 1976 (1997).

[10] P. Sigmund and C. Claussen, J. Appl. Phys. **52**, 990 (1981).

[11] P. C. Zalm and L. J. Beckers, Philips J. Res. **39**, 11 (1984).

[12] G. Carter and J. S. Colligon, *Ion Bombardment of Solids* (American Elsevier, New York, 1968).

[13] *Handbook of Chemistry and Physics*, 56th ed., edited by R. C. Weast (Chemical Rubber Company, Cleveland, OH, 1975).

[14] K. A. Gschneidner, Solid State Phys. **16**, 275 (1964).

[15] J. E. Mahan, *Physical Vapor Deposition of Thin Films* (Wiley, New York, 2000).

[16] Ch. Steinbrüchel, Appl. Phys. A 36, 37 (1985).

[17] N. C. Barford, *Experimental Measurements: Precision, Error, and Truth*, 2nd edition (Wiley, New York, 1985), p. 74.